Monthly Notices
of the
ROYAL ASTRONOMICAL SOCIETY

MNRAS **431,** 3177–3188 (2013)
Advance Access publication 2013 April 9

doi:10.1093/mnras/stt403

Relaxation of *N*-body systems with additive $r^{-\alpha}$ interparticle forces

PierFrancesco Di Cintio,[1]⋆ Luca Ciotti[2] and Carlo Nipoti[2]

[1]*Max Planck Institute for the Physics of Complex Systems, Nöthnitzer Straße 38, D-01187 Dresden, Germany*
[2]*Department of Physics and Astronomy, Bologna University, viale Berti-Pichat 6/2, I-40127 Bologna, Italy*

Accepted 2013 March 2. Received 2013 March 1; in original form 2013 January 21

ABSTRACT

In Newtonian gravity the final states of cold dissipationless collapses are characterized by several structural and dynamical properties remarkably similar to those of observed elliptical galaxies. Are these properties a peculiarity of the Newtonian force or a more general feature of long-range forces? We study this problem by means of *N*-body simulations of dissipationless collapse of systems of particles interacting via additive $r^{-\alpha}$ forces. We find that most of the results holding in Newtonian gravity are also valid for $\alpha \neq 2$. In particular, the end-products are triaxial and never flatter than an E7 system, their surface density profiles are well described by the Sérsic law, the global density slope–anisotropy inequality is obeyed, the differential energy distribution is an exponential over a large range of energies (for $\alpha \geq 1$), and the pseudo-phase-space density is a power law of radius. In addition, we show that the process of virialization takes longer (in units of the system's dynamical time) for decreasing values of α, and becomes infinite for $\alpha = -1$ (the harmonic oscillator). This is in agreement with the results of deep Modified Newtonian Dynamics collapses (qualitatively corresponding to $\alpha = 1$) and it is due to the fact that the force becomes more and more similar to the $\alpha = -1$ case, where, as well known, no relaxation can happen and the system oscillates forever.

Key words: methods: numerical – galaxies: formation – galaxies: kinematics and dynamics.

1 INTRODUCTION

One of the most striking properties of elliptical galaxies is the remarkable quasi-homology of their surface brightness profiles, described by the so called Sérsic model, a generalization of the de Vaucouleurs $R^{1/4}$ model (see e.g. Caon, Capaccioli & D'Onofrio 1993; Andredakis, Peletier & Balcells 1995; Courteau, de Jong & Broeils 1996; Graham & Colless 1997; Prugniel & Simien 1997; Graham 1998; Trujillo, Graham & Caon 2001; Bertin, Ciotti & Del Principe 2002; see also Ciotti 2009 and references therein). Albeit minor (but important) departures from the Sérsic model are common, overall the profiles on large scale are very well represented by the Sérsic law. What is the origin of such regularity? *N*-body numerical simulations revealed that cold dissipationless and collisionless collapses lead to virialized end-states described almost perfectly by $R^{1/4}$ profiles (e.g. van Albada 1982; Londrillo, Messina & Stiavelli 1991). More recently, it has been shown that collapses in pre-existing dark matter haloes are also well described by the Sérsic profile, with a wide range of values of the Sérsic index (Nipoti, Londrillo & Ciotti 2006a,b, hereafter N06ab). In addition, it is also known that the Sérsic family is characterized by an exponential differential energy distribution, over a large range of accessible energies (e.g. Binney 1982; Ciotti 1991). These results can be understood in terms of the physics of violent relaxation in collisionless collapses (e.g. Lynden-Bell 1967; Bertin & Stiavelli 1984; Bertin & Trenti 2003; Trenti & Bertin 2005; Trenti, Bertin & van Albada 2005). Finally, it has been proved analytically that in Newtonian gravity a large class of spherically symmetric equilibrium systems are characterized by the so-called global density slope–anisotropy inequality (hereafter GDSAI; see Ciotti & Morganti 2010a,b; van Hese, Baes & Dejonghe 2011; An, van Hese & Baes 2012; see also An & Evans 2006), a constraint between their anisotropy and density profiles. Numerical simulations suggest that the GDSAI may be a much more general result, holding true also for the final states of dissipationless collapses (see e.g. Hansen & Moore 2006).

Due to the relevance of these results for the understanding of the process of collisionless relaxation, a natural question arises about their apparent universality. In particular, are the Sérsic law, the associated differential exponential energy distribution and the GDSAI peculiar features of Newtonian gravity or are they more general properties of the virialized final states of *N*-body collapses in which the particles interact with long-range forces? Preliminary results seem to support the second possibility. For example, it is known that the end-products of cold collapses in Modified Newtonian Dynamics (MOND; Bekenstein & Milgrom 1984) also produce final systems described remarkably well by the Sérsic law (Nipoti, Londrillo & Ciotti 2007a, hereafter N07a; Ciotti, Nipoti & Londrillo 2007). However, the *N*-body MOND simulations have also shown that the oscillations leading to relaxation last more (in units of the dynamical time of the system) than in the equivalent Newtonian system (see e.g. N07a; Nipoti, Londrillo & Ciotti 2007b).

⋆ E-mail: pdicint@pks.mpg.de

Moreover, Barber et al. (2012) found indications that the GDSAI may be a common property of MONDian virialized systems. We recall that the force law in the MOND weak field limit (or deep-MOND, hereafter dMOND) regime is qualitatively similar to a force decreasing with distance as $1/r$.

Additional indications in this direction come from the preliminary analysis of Di Cintio (2009, hereafter DC09) and Di Cintio & Ciotti (2011, hereafter DCC11), who investigated the relaxation of a system of spherical shells interacting via a long-range $r^{-\alpha}$ force law, in analogy with similar studies performed in Newtonian gravity (Hénon 1964; Takizawa & Inagaki 1997; Youngkins & Miller 2000) and MOND (Sanders 1998, 2008; Malekjani, Rahvar & Haghi 2009; Malekjani, Haghi & Jassur 2012). In DCC11, we focused on the time evolution of the virial ratio and of the differential energy distribution. Among the main results, we confirmed the expectation that the process of relaxation, independently of the value of α (with the exception of $\alpha = -1$), consists in a first phase of violent collapse, followed by a longer, gentle phase of dynamical mixing. Remarkably, small values of α correspond to larger and long-lasting virial oscillations, confirming the dMOND results (N07a). However, the final states of shell systems are only poorly described by an exponential differential energy distribution. This is not surprising since the enforced spherical symmetry reduces the number of degrees of freedom available for energy exchanges during virialization.

Prompted by these preliminary results, here we explore further the problem following the collapse and virialization of fully three-dimensional N-body systems of particles interacting with radial forces proportional to a power law of the mutual separation, $r^{-\alpha}$. This approach is not new, and here we recall the study of quasi-stationary states (Gabrielli, Joyce & Marcos 2010; Marcos, Gabrielli & Joyce 2012) and of Yukawa-like gravity (Moffat & Sokolov 1996 and references therein; see also Brandao & de Araujo 2012). For the simulations, we developed a direct N-body code, exploiting the force additivity. Note that for general forces, more sophisticated methods, based on the expansion in orthogonal functions of the potential, are not available, as the analogue of the Poisson equation does not exist. In our case, the considered forces, even though additive, are described by *non-local* operators, i.e. the density at a given point cannot be expressed as a simple differential operator of the potential at that point. In fact, the potentials associated with $r^{-\alpha}$ forces are the well-known *Riesz potentials*, and the analogue of the Poisson equation involves the so-called fractional Laplacian (e.g. Stein 1970). Remarkably, for this specific cases, the potential can be expressed in terms of Gegenbauer polynomials in turn expressible with an addition theorem on spherical harmonics, so that in principle a multipole-based Treecode can be realized (see Srinivasan, Mahawar & Sarin 2005). Note that MOND is a non-linear but *local* theory.

The paper is organized as follows. In Section 2, we introduce the most important integral identities that will be used to study the results of the simulations, while in Section 3, the numerical code and the set-up of the initial conditions are presented. In Section 4, the virialization process and the structure and the dynamical properties of the virialized final states are presented and discussed as a function of α. The main results are finally summarized in Section 5.

2 SETTING THE STAGE

We integrate numerically the equations of motion for an initially spherical system consisting of N particles of identical mass m, mutually interacting with central long-range forces, obeying the superposition principle. In particular, the acceleration at $\boldsymbol{r}_i$ due to a particle of mass m_j at $\boldsymbol{r}_j$ is

$$\boldsymbol{a}_{ji} = -Gm_j \times \frac{\boldsymbol{r}_i - \boldsymbol{r}_j}{||\boldsymbol{r}_i - \boldsymbol{r}_j||^{\alpha+1}}, \tag{1}$$

where $||\ ||$ is the standard Euclidean norm and G is the force constant. The associated potential is

$$\phi_{ji} = Gm_j \times \begin{cases} \dfrac{||\boldsymbol{r}_i - \boldsymbol{r}_j||^{1-\alpha}}{1-\alpha}, & \alpha \neq 1, \\ \ln ||\boldsymbol{r}_i - \boldsymbol{r}_j||, & \alpha = 1, \end{cases} \tag{2}$$

with $\boldsymbol{a}_{ji} = -\nabla_i \phi_{ji}$. Note that for $\alpha = 2$ we recover the Newtonian gravity, for $\alpha = -1$ Hooke's harmonic force and finally $\alpha = 1$ is the additive[1] analogue of the dMOND regime in which the MOND force behaves qualitatively as $1/r$. Some authors (e.g. Chavanis 2008; Bouchet, Gupta & Mukamel 2010) introduce the nomenclature of *weak* long-range interactions and *strong* long-range interactions depending on whether the force vanishes or diverges for $r \to +\infty$; here, we label them as *gravity like* ($\alpha > 0$) or *harmonic oscillator like* ($\alpha \leq 0$). The forces in equation (1) can also be divided in two families depending on the confining nature of their potential, separated by the case $\alpha = 1$, when the potential diverges for zero and infinite separation. For $\alpha \geq 1$, the total energy of a particle may be positive or negative, while it is always positive for $\alpha < 1$ (having assumed zero potential energy for a system collapsed at the origin). Particles can escape only from systems with $\alpha > 1$, while bound particles have negative energies.

In order to keep track of the process of virialization for each simulation, we follow the evolution of the virial ratio

$$\eta = \frac{2K}{|W|}, \tag{3}$$

where

$$K = \sum_{i=1}^{N} \frac{m_i v_i^2}{2} \tag{4}$$

is the total kinetic energy of the system, and

$$W = -\int \rho(\boldsymbol{x}) \langle \boldsymbol{x}, \nabla\phi \rangle \mathrm{d}^3\boldsymbol{x} = \sum_{j\neq i=1}^{N} m_i \langle \boldsymbol{x}_i, \boldsymbol{a}_{ji} \rangle \tag{5}$$

is the virial function, so that the virial theorem reads $2K = -W$. Note that the condition $j \neq i$ in equation (5) is required for $\alpha > 0$; however, this condition can be extended without loss of generality also to $\alpha \leq 0$, due to the fact that the self-force vanishes. Note also that convergence of the integral in equation (5) requires $\alpha < 3$. We recall that in general W is *not* the total potential energy

$$U = \frac{1}{2}\int \rho(\boldsymbol{x})\phi(\boldsymbol{x})\,\mathrm{d}^3\boldsymbol{x} = \frac{1}{2}\sum_{j\neq i=1}^{N} m_i \phi_{ji}, \tag{6}$$

but for $\alpha \neq 1$ it is proportional to it, being

$$W = (\alpha - 1)U. \tag{7}$$

Note that $U = 0$ when the system is dispersed at infinity for $\alpha > 1$, while $U = 0$ when the system is collapsed at the origin for $\alpha < 1$. In the $\alpha = 1$ case, the reference state must be fixed with the particles at finite (but non-zero) separation. The case $\alpha = 1$, corresponding

[1] Recently, Milgrom (2010) proposed a quasi-linear formulation of MOND called QuMOND. We stress that the $\alpha = 1$ case studied here is not QuMOND.

to the logarithmic potential (i.e. to dMOND-like force), is peculiar, as from equations (1) and (5) one obtains[2]

$$W = -\frac{G}{2}\sum_{i\neq j=1}^{N} m_i m_j, \tag{8}$$

i.e. W remains constant during the virialization. Remarkably, it can be shown analytically that the virial function is time independent also in dMOND, even though the field equation is not linear and the force is in general neither radial nor strictly proportional to $1/r$ (N07a; for the special case of spherical systems see Gerhard & Spergel 1992). As the total energy $E = K + U$ is conserved for all values of α, oscillations in K are always associated with oscillations in U, so that for $\alpha \neq 1$ equation (7) and the Lagrange–Jacobi identity $\ddot{I} = 2(2K + W)$ (e.g. Ciotti 2000) show that the time dependence of the moment of inertia of the system is due to the combined effects of K and U. For $\alpha = 1$ instead only the kinetic energy changes during the virialization. Finally, for a dissipationless collapse, starting from cold initial conditions ($K_{\rm in} = 0$), it is easy to prove that the value of the equilibrium wirial function ($W_{\rm fin}$) is related to the initial potential energy $U_{\rm in}$ by

$$W_{\rm fin} = \frac{2W_{\rm in}}{3-\alpha} = \frac{2(\alpha-1)(U_{\rm in} - K^e_{\rm fin})}{3-\alpha}, \quad (\alpha \neq 1). \tag{9}$$

where $K^e_{\rm fin}$ is the asymptotic energy of the possible escapers. In the identity above, it is assumed that the escapers are fully dispersed, i.e. that their gravitational energy is small and that $W_{\rm fin}$ is the virial function of the remnant. Not also that in the cases with $\alpha < 1$ no escape is possible, so that equation (9) holds rigorously with $K^e_{\rm fin} = 0$ (provided equilibrium could be attained), and $W_{\rm fin}$ refers to the whole system. We used equation (9) as a test for the simulations.

3 THE SIMULATIONS

3.1 The *N*-body code

In order to compare the process of virialization of systems with different values of α, we introduce the time-scale t_* from the relation

$$\frac{GMt_*^2}{2r_*^{\alpha+1}} = 1, \tag{10}$$

where r_* (the length-scale) is the half-mass radius of the density distribution at $t = 0$, and $M = Nm$ is the total mass of the system (see also DCC11); the natural velocity scale becomes

$$v_* \equiv \frac{r_*}{t_*}. \tag{11}$$

Setting $\boldsymbol{x} \equiv \boldsymbol{r}/r_*$ and $\tau \equiv t/t_*$, the dimensionless equations of motion for the particle i become

$$\frac{{\rm d}^2\boldsymbol{x}_i}{{\rm d}\tau^2} = -\frac{2}{N}\sum_{j\neq i=1}^{N} \frac{\boldsymbol{x}_i - \boldsymbol{x}_j}{||\boldsymbol{x}_i - \boldsymbol{x}_j||^{\alpha+1}}. \tag{12}$$

We note that, as all the presented results are scaled to the dynamical time t_*, the specific value of G does not affect the conclusions. The code used for the simulations is a direct code, with the consequent limitations on the number of particles that can be used: as a rule we adopt $N = 25\,000$. In the case of gravity-like forces ($\alpha > 0$), the divergence of the force when the interparticle separation tends to zero is cured with the introduction of the softening length ϵ (e.g. Dehnen 2001), so that equations (1) and (2) are replaced by their softened expressions

$$\boldsymbol{a}^{\rm soft}_{ji} = -Gm_j \times \frac{\boldsymbol{r}_i - \boldsymbol{r}_j}{\left(||\boldsymbol{r}_i - \boldsymbol{r}_j||^2 + \epsilon^2\right)^{\frac{\alpha+1}{2}}}, \tag{13}$$

$$\phi^{\rm soft}_{ji} = Gm_j \times \begin{cases} \dfrac{\left(||\boldsymbol{r}_i - \boldsymbol{r}_j||^2 + \epsilon^2\right)^{\frac{1-\alpha}{2}}}{1-\alpha}, & \alpha \neq 1; \\ \ln\sqrt{||\boldsymbol{r}_i - \boldsymbol{r}_j||^2 + \epsilon^2}, & \alpha = 1. \end{cases} \tag{14}$$

The optimal ϵ is chosen as follows: the density profile of the initial conditions is divided in spherical shells of radius R_i and thickness δR_i, and the minimum interparticle distance d_i within each shell is computed. A value ϵ_i is obtained by comparing the acceleration $a^{\rm soft}(d_i, \epsilon_i)$ of a pair with separation d_i with $a^{\rm soft}_i(\epsilon_i)$, the acceleration of a random particle of the shell due to all the other particles of the system. The value of ϵ_i is chosen so that $a^{\rm soft}_i(\epsilon_i) = a^{\rm soft}(d_i, \epsilon_i)$. As optimal ϵ, we take the maximum ϵ_i. We verified that with such choice, independently of α, the softened acceleration of a particle at a large distance from the centre of mass of the system differs by less than 0.01 per cent from the non-softened acceleration. The equations of motion are integrated using a standard second-order leapfrog method both with constant and adaptive time step Δt. In the second case, $\Delta t = \min(\Delta t_i)$, where $\Delta t_i = \min(\Delta t_{1i}, \Delta t_{2i}, \Delta t_{3i})$, and

$$\Delta t_{1i} \equiv \frac{||\Delta \boldsymbol{r}_i||}{||\Delta \boldsymbol{v}_i||}, \quad \Delta t_{2i} \equiv \frac{m_i||\Delta \boldsymbol{r}_i||^2}{||\Delta \boldsymbol{J}_i||}, \quad \Delta t_{3i} \equiv \sqrt{\frac{m_i||\Delta \boldsymbol{r}_i||^2}{|\Delta E_i|}}. \tag{15}$$

Here, $\Delta \boldsymbol{r}_i$, $\Delta \boldsymbol{v}_i$, ΔE_i and $\Delta \boldsymbol{J}_i$ are the variation of position, velocity, energy and angular momentum of the ith particle in the previous time steps.

3.2 Initial conditions

In the present exploration, the force exponent spans the range $-5/2 \leq \alpha \leq 5/2$, and the initial conditions are characterized by values of the virial ratio $0 \leq \eta_0 = 2K_{\rm in}/|W_{\rm in}| \leq 0.5$. The N particles are distributed in space with a standard rejection technique. In the first family, used to study the evolution of cuspy initial conditions, we adopt the Hernquist (1990) density profile

$$\rho(r) = \frac{Ma}{2\pi r(r+a)^3}, \tag{16}$$

where M is the total mass, $a = r_*(\sqrt{2}-1)$ is the scale radius and r_* is the half-mass radius. In the second family of initial conditions, characterized by a flat core, we use the Plummer (1911) density profile

$$\rho(r) = \frac{3Ma^2}{4\pi\left(r^2+a^2\right)^{5/2}}; \tag{17}$$

in this case, $a = r_*\sqrt{2^{2/3}-1}$. We then extract the initial velocities of the particles from a position-independent Gaussian distribution, with the velocity dispersion tuned as to obtain the desired initial virial ratio η_0. The results are independent of the values of M and a, which do not appear in the dimensionless equations of motion (equation 12), so for each of the two families we explore the two-dimensional parameter space defined by the pair (α, η_0). We note that similar initial conditions have been used recently for the numerical study of violent relaxation in Newtonian gravity (e.g. Visbal,

[2] Note that in the case of a continuous density distribution with $\alpha = 1$ and total mass M, $W = -GM^2/2$, and this is not the limit of equation (8) for $N \to \infty$ and $m = M/N$.

Loeb & Hernquist 2012; Sylos Labini 2013). All the simulations presented in this paper were performed on a cluster of LINUX HP® Z700 workstations, and each run (on a single processor) lasted for ≈4 d when extended up to 50 t_*.

3.3 Analysis of the numerical outputs

The numerical outputs are used not only to study the dependence of the virialization process on the force law but also to investigate the structural and dynamical properties of the final states. We assume that the system has reached its final state when the amplitude of the oscillations of η becomes smaller than 10^{-4} (which typically occurs at $t \approx 30 t_*$). Following Nipoti, Londrillo & Ciotti (2002) and Meza & Zamorano (1997), we compute the second-order tensor[3]

$$I_{ij} \equiv m \sum_{k=1}^{N} r_i^{(k)} r_j^{(k)} \tag{18}$$

for the particles inside the sphere of radius r_{85} containing the 85 per cent of the total mass of the system, where r_i are the Cartesian components of the position vector in the reference frame with origin in the centre of mass. The matrix I_{ij} is diagonalized iteratively, requiring the percentage difference of the largest eigenvalue between two iterations to be smaller than 10^{-3}. This procedure requires on average 10 iterations, and we call $I_1 \geq I_2 \geq I_3$ the three eigenvalues. We finally apply a rotation to the system in order to have the three eigenvectors oriented along the coordinate axes. For of a heterogeneous ellipsoid of semi-axes a, b and c, we would obtain $I_1 = Aa^2$, $I_2 = Ab^2$ and $I_3 = Ac^2$, where A is a constant depending on the density profile. Consistently, for the end-products we define $b/a = \sqrt{I_2/I_1}$ and $c/a = \sqrt{I_3/I_1}$, so that the ellipticities in the principal planes are $\epsilon_1 = 1 - \sqrt{I_2/I_1}$ and $\epsilon_2 = 1 - \sqrt{I_3/I_1}$.

It is known (see e.g. van Albada 1982; Londrillo et al. 1991; Trenti et al. 2005; N06a) that the end-products of Newtonian dissipationless collapses starting from cold initial conditions (and also of MOND dissipationless collapses, see N07a) have surface density profiles well described by the Sérsic law

$$\Sigma(R) = \Sigma_e e^{-b\left[\left(\frac{R}{R_e}\right)^{1/m} - 1\right]}, \tag{19}$$

where $b \simeq 2m - 1/3 + 4/405m$ (Ciotti & Bertin 1999) and Σ_e is the projected mass density at effective radius R_e, the radius of the circle containing half of the projected mass. In practice, in our analysis, we circularize the projected density in the three principal planes of the virialized systems, and by particle count we determine the corresponding pair (R_e, Σ_e), so that from equation (19) we obtain the best-fitting m. In this way for each simulation we determine three sets of (Σ_e, R_e, m) and we then chose randomly one of them, being the others in general qualitatively similar.

In the same spirit as previous works (DC09; DCC11), we focus on different indicators of relaxation, such as the evolution of the virial ratio and of the phase-space sections (r, v_r). We also study the final differential energy distribution $n(E)$, defined by the relation

$$\int_{E_{\min}}^{E_{\max}} n(E)\, \mathrm{d}E = N \tag{20}$$

(e.g. Binney & Tremaine 2008). Finally, we construct the so-called pseudo-phase-space density of the final states and we check if they obey the GDSAI, as described in Section 4.3.

[3] Notice that I_{ij} is *not* the inertia tensor, which is given instead by $\mathrm{Tr}(I_{ij})\delta_{ij} - I_{ij}$.

3.4 Testing the code

As a first set of numerical experiments, we determined the optimum choice of the softening length and of the time step to be used in the simulations. Following the procedure described in Section 3.1, we found that, independently of α, $\epsilon \simeq 10^{-2} r_*$ guarantees not only numerical accuracy of the results (with energy conservation better than 3 per cent at virialization in the worst cases, and usually better than the 0.5 per cent), but also acceptable computational times. In addition, comparing the evolution of collapses starting from identical initial conditions with adaptive or fixed time steps, we found that a fixed time step $\Delta t \simeq 10^{-2} t_*$ guarantees a good balance between computational time and energy and total angular momentum conservation independently of the value of α and of the initial profile, so we adopt this criterion for all the simulations.

We tested our direct code in the Newtonian case against several well-established results of numerical simulations of cold collapses obtained with the tree-code FVFPS (Londrillo, Nipoti & Ciotti 2003), as well as in the Newtonian limit with the particle-mesh MOND code N-MODY (Londrillo & Nipoti 2009). In particular, we performed collapses for different initial density profiles and values of the virial ratio. We fit the final surface density profile with the Sérsic law over the radial interval $0.3R_e - 10R_e$. As shown in Fig. 1 (left-hand panel) the resulting values of m range from $\simeq$2 for the hottest initial condition ($\eta_0 = 0.5$) to $\simeq$4 for the cold collapse ($\eta_0 = 0$). Over the radial range here considered, the final profiles are indistinguishable from those obtained by N06a for comparable values of the initial virial ratio ($0 \leq \eta_0 \leq 0.2$). As can be seen from Fig. 2 the final states, for both Hernquist and Plummer initial profiles, are roughly spherical for $\eta_0 > 0.1$ and prolate ($c/a \simeq b/a \simeq 0.5$) for $\eta_0 \leq 0.1$, consistent with the results of N06a, which indicates that colder systems are more prone to undergo instabilities that perturb significantly their initial shape. Finally, the tests confirm that after virialization $n(E)$ is well described over a broad range of energies by an exponential function. Remarkably, slightly bimodal final differential energy distributions characterize the systems starting from hotter initial conditions (Fig. 1, right-hand panel) as seen in analogous plots of previous papers (fig. 2 in N06b and fig. 8 in Londrillo et al. 1991).

4 RESULTS

4.1 The relaxation process

One of the motivations of this study is to elucidate the reason of the long relaxation time (in units of their dynamical time) of dMOND systems when compared to the same quantity for Newtonian systems. A simple measure of the relaxation effectiveness can be obtained considering the number and the decay rate of the major oscillations of the virial ratio η. In Fig. 3, we show the evolution of η as a function of the dimensionless time τ for cold ($\eta_0 = 0$) Hernquist initial conditions with different values of α. The top panel illustrates the evolution for the family of gravity-like forces. The similarity with the results obtained with the shell models (fig. 1 in DCC11) is remarkable: a decrease of α leads to a higher value of η at the first peak, and to a longer series of virial oscillations of decreasing amplitude. Curiously, for $\alpha = 1$ the amplitude of the virial oscillations increases again at large times, similarly to dMOND collapses (N07a; Ciotti et al. 2007), confirming that dMOND behaves qualitatively as the $1/r$ force when considering a system not deviating too much from spherical shape, reinforcing the previous result of the long relaxation times of N-body systems governed by the non-linear field equation of MOND. We interpret the large peak

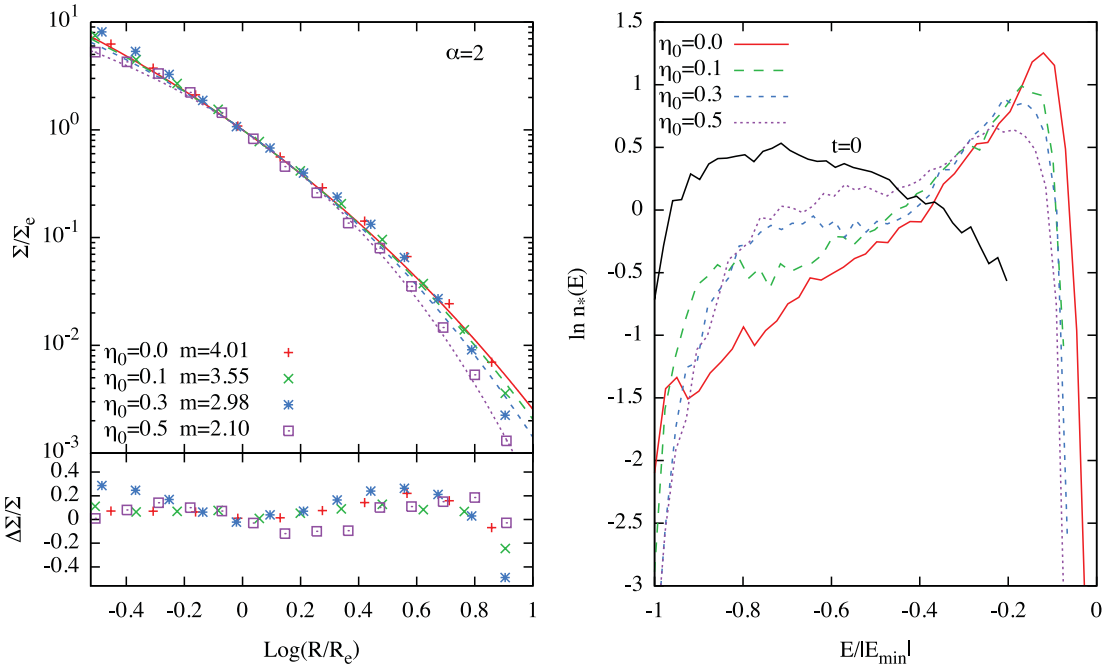

Figure 1. Newtonian ($\alpha = 2$) tests for Plummer initial conditions with $0 \leq \eta_0 \leq 0.5$. Left: projected density profiles for the final states at 50 t_* (dots), and their best-fitting Sérsic profiles (lines); residuals are also shown. Right: normalized differential energy distribution $n_*(E) = n(E)/N$ for the final states. The black solid line represents $n_*(E)$ for the initial condition with $\eta_0 = 0$; note that $E_{\rm min}$ depends on the specific realization.

values of η for small α as due to the fact that the force is stronger on large scales, and that the systems with low α collapse more as a whole, consistently with the force being more similar to the harmonic oscillator case. It is important to recall that in the Newtonian case a spherical homogeneous shell does not exert any force inside, while inside a shell the force is directed outwards for $\alpha > 2$, and the opposite happens for $\alpha < 2$ (e.g. DCC11). Therefore, when $\alpha > 2$ the external regions act *against* the collapse, while for $\alpha < 2$ also the external regions of the system contribute more and more to the collapse.

The results for collapses driven by harmonic-like forces are shown in the bottom panel of Fig. 3. Note how the virial ratio oscillates with peak values of η significantly larger, and more regular oscillations than in the gravity-like cases. As expected, in the $\alpha = -1$ case no relaxation takes place, since the whole system behaves as a single harmonic oscillator (e.g. Lynden-Bell & Lynden-Bell 2008, see also equation 12). In particular, in a system of harmonic oscillators starting at rest, all the particles cross the centre simultaneously, so that $|W| \rightarrow 0$ while $K \rightarrow -E$, causing η to diverge. For the reasons described above, in the superharmonic case ($\alpha < -1$), the first peak of η is reached at earlier times for decreasing α. However, the peak values decrease, due to phase mixing which forbids all the particles to cross the centre simultaneously. Cases with η_0 slightly larger than 0, and for the Plummer initial conditions, are not shown, being qualitatively the same. In general, large values of η_0 correspond to small amplitudes of the first peak of η.

The long lasting virial oscillations for forces close to the harmonic oscillator are associated with a poorer mixing in phase space. Such behaviour is evident from the evolution in the phase-space section (r, v_r) defined as radial position and radial velocity. In Fig. 4, we show snapshots of the phase space at 1, 10 and 50 t_* for $\alpha = -2, -1$, 1, 2. Consistently with the findings of DCC11 (where the narrower interval of $1 \leq \alpha \leq 2$ was studied), larger values of α show a more efficient phase mixing with respect to systems with $\alpha \leq 0$. Again, the similarity with the plots in N07a (their fig. 4) and Ciotti et al. (2007, their figs 2 and 3) is remarkable. One may speculate that the coherent structures in phase space that persist at large times (in units of t_*) are akin to the so-called *phase-space holes* reported by some authors (Mineau, Feix & Rouet 1990; Joyce & Worrakitpoonpon 2011; Teles, Levin & Pakter 2011) in the context of the one-dimensional infinite sheet model, where the mixing is quite poor. It must be pointed out that the poorer mixing in Newtonian gravity in lower dimensions is essentially due to the smaller number of degrees of freedom that are involved in the relaxation rather than a different exponent in the force law (see e.g. Kandrup 1989). As already remarked, the efficiency of phase mixing is non-monotonic with α, with no mixing for $\alpha = -1$.

4.2 Structural properties of the end-products

The triaxiality of the final states of the collapses is shown in Fig. 2 where we plot the values of the axial ratios b/a and c/a of the end-products at 50 t_*, for representative values of α and for increasing values of η_0. In general, the Newtonian behaviour is confirmed, in the sense that at fixed α triaxiality is more pronounced for small values of η_0, for both Plummer and Hernquist initial conditions. Again, the only exception is the $\alpha = -1$ force, when the systems retain their spherical shapes, consistently with their orbital structure. For given η_0, the triaxiality as a function of α shows characteristic non-monotonic trend especially visible in the bottom panel of Fig. 2 for $\eta_0 = 0$ and $\eta_0 = 0.1$. For decreasing α the flattening increases, reaches a maximum, and then decreases again. The maximum values of the triaxiality (the minimum values of b/a and c/a) are obtained for $1 \leq \alpha \leq 2$ when $0 \leq \eta_0 \leq 0.1$, with a quite clear correlation between α and η_0. Remarkably, no models are found to be flatter than an elliptical galaxy E7 (i.e. $c/a \geq 0.3$), thus leading to conjecture that this limit may hold more generally than just in Newtonian gravity.

In analogy with the case of Newtonian collapses, we fitted the final projected density profile with the Sérsic law as described in

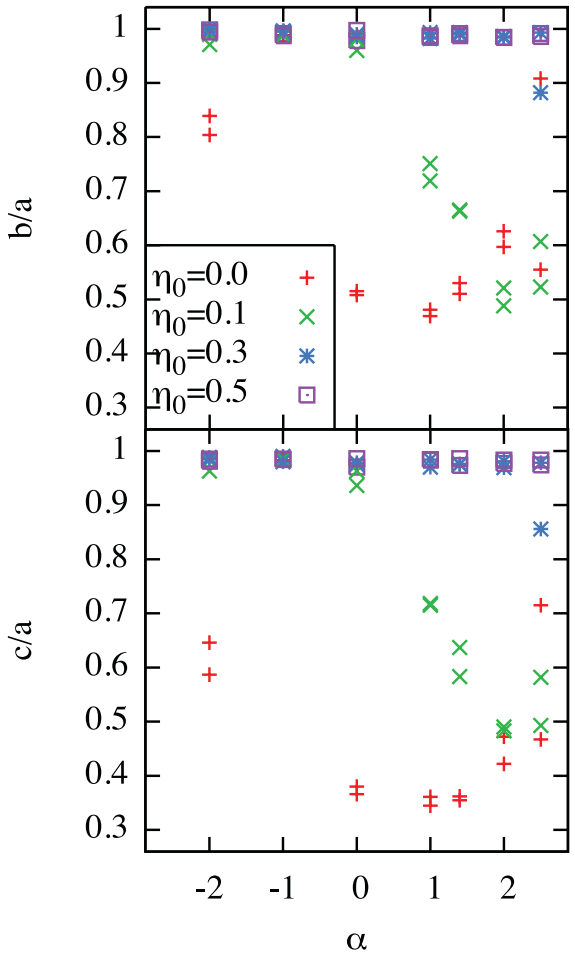

Figure 2. Final axial ratios as a function of the force exponent α, for Hernquist and Plummer initial conditions with different values of η_0. Note that how for each value of η_0, the results are almost identical independently of the initial density profile. In the harmonic oscillator case ($\alpha = -1$), the systems retain their spherical shape.

Section 3.3. In general, we find that the Sérsic law provides a good description of most of the final states for both Plummer and Hernquist initial conditions. More quantitatively, in the left-hand panel of Fig. 5 we show the end-state of the collapse of a perfectly cold Hernquist initial condition. The main result is a quite well-defined dependence of the Sérsic index m on α, with large values of m associated with large values of α. In practice, gravity-like forces produce more peaked density profiles than harmonic like forces. The $\alpha = -1$ case is not shown, as the profile collapses and expands self-similarly. For other values of α, percentual deviations of the data from the fits are well within the 20 per cent. The model with the largest deviations is the superharmonic one with $\alpha = -2$ and $m \simeq 2.4$. The dependence of the final states on η_0 is shown in Fig. 6. In general, hotter initial conditions lead to smaller values of m, independently of α (for the Newtonian case see Fig. 1, left-hand panel). Moreover, the largest deviations from the best fit are again produced by the superharmonic $\alpha = -2$ force, while the $\alpha = 1$ case is remarkably similar to the dMOND results of N07a.

For completeness, in Fig. 7 we also show the three-dimensional (angle-averaged) density profiles of the end-products of cold ($\eta_0 = 0$) Plummer initial conditions. As apparent, and in agreement with the projected density profiles, higher values of α corresponds to more peaked final density profiles, while for $\alpha = -1$ the normalized profile does not change.

4.3 The differential energy distribution, the pseudo-phase-space density and the GDSAI of the end-products

In addition to their structural properties, the virialized final states of collapses are usually also studied from the point of view of the phase-space properties. Here, following a well-established approach, we focus on their differential energy distribution, on the radial trend of the so-called pseudo-phase-space density, and finally on the density–slope inequality.

In Fig. 8 we show the final differential energy distribution $n(E)$ for $-2 \leq \alpha \leq 2.5$, and for different values of η_0. Each distribution

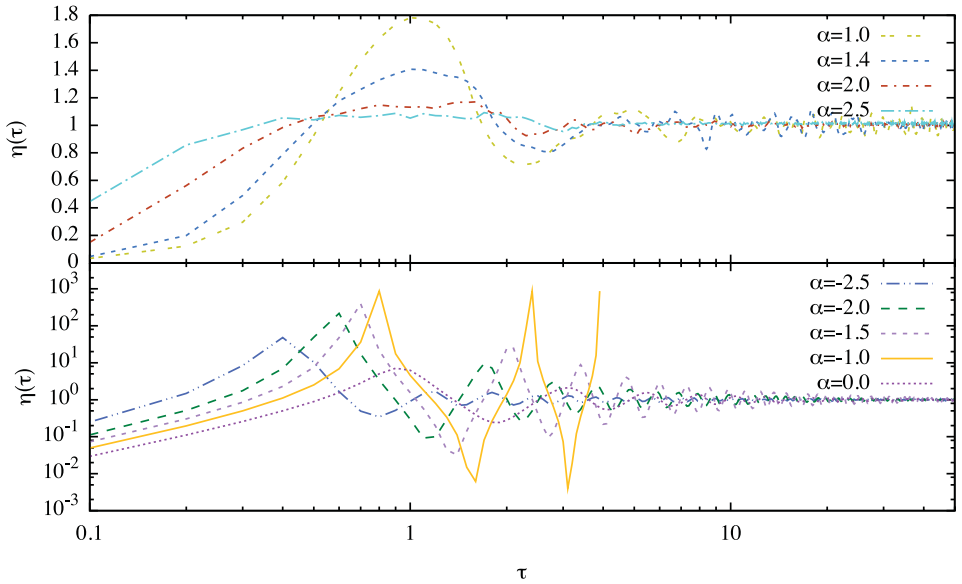

Figure 3. Time evolution of the virial ratio η for cold ($\eta_0 = 0$) Hernquist initial conditions with different values of α. Upper panel: gravity-like forces ($\alpha > 0$). Lower panel: harmonic oscillator-like forces ($\alpha \leq 0$). For clarity, the unrelaxing case of the harmonic force ($\alpha = -1$, solid line) has been plotted only up to the third peak of η.

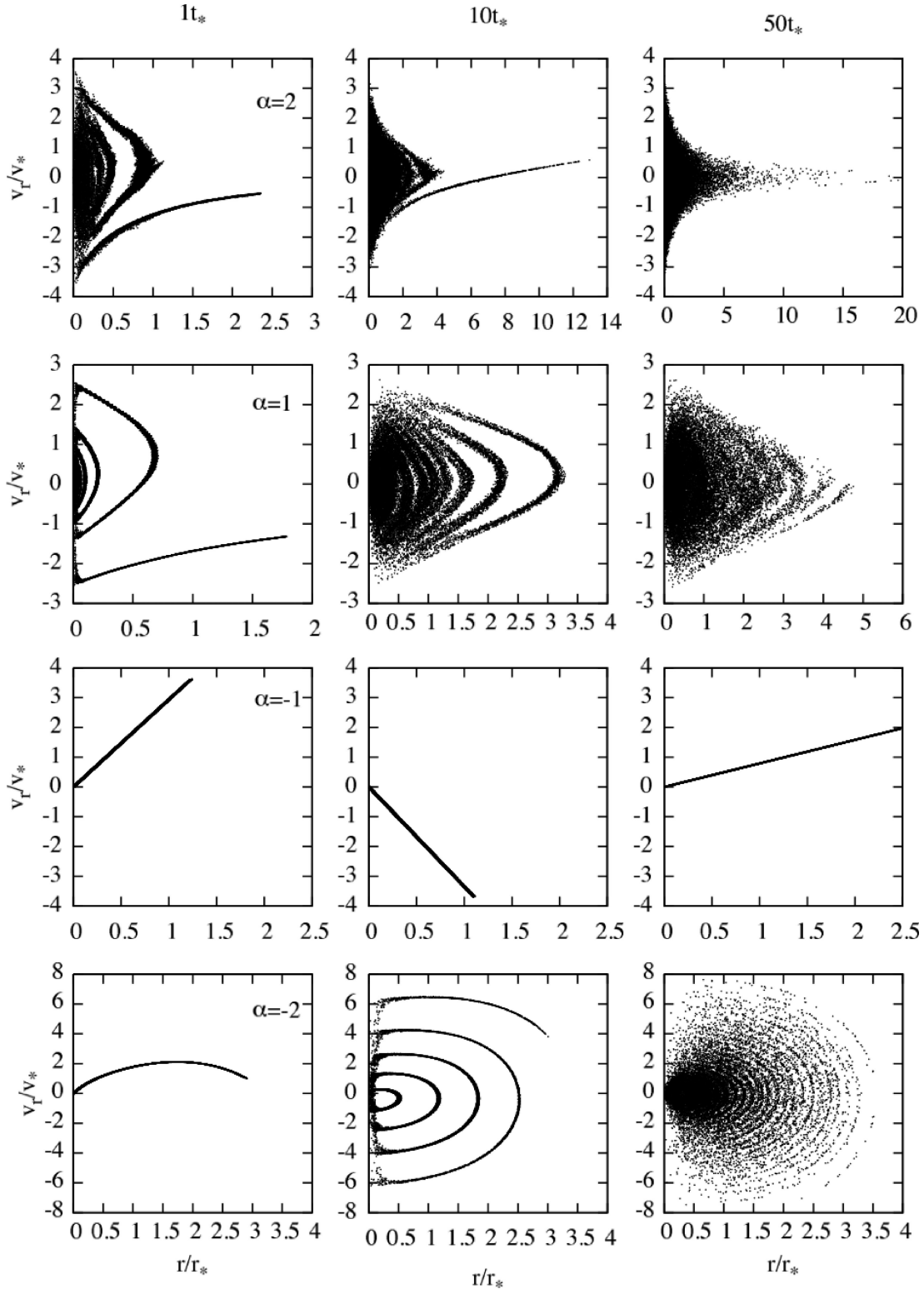

Figure 4. The evolution of phase-space sections (r, v_r) for Hernquist initial conditions with $\eta_0 = 0$, and $-2 \leq \alpha \leq 2$. As expected, no mixing is acting on the harmonic-oscillator case ($\alpha = -1$, where the straight line rotates clockwise and each point of it describes similar ellipses), while mixing appears again in the superharmonic case ($\alpha = -2$). The characteristic time and length-scales, t_* and r_*, are related as given by equation (10).

is normalized to the total number of particles, and the energy range to $E_{\max}$ (for $\alpha \leq 1$) and to $|E_{\min}|$ (for $\alpha > 1$) of the final states. The initial conditions with $\eta_0 = 0$ are represented by the heavy solid lines. The first important and general feature is that $n(E)$ is peaked at high energies for $\alpha > 1$ (see also Fig. 1, right-hand panel, for the Newtonian case). In practice, the virialized final states of systems with gravity-like forces allowing for escape are mainly supported by loosely bound particles (e.g. Binney 1982;

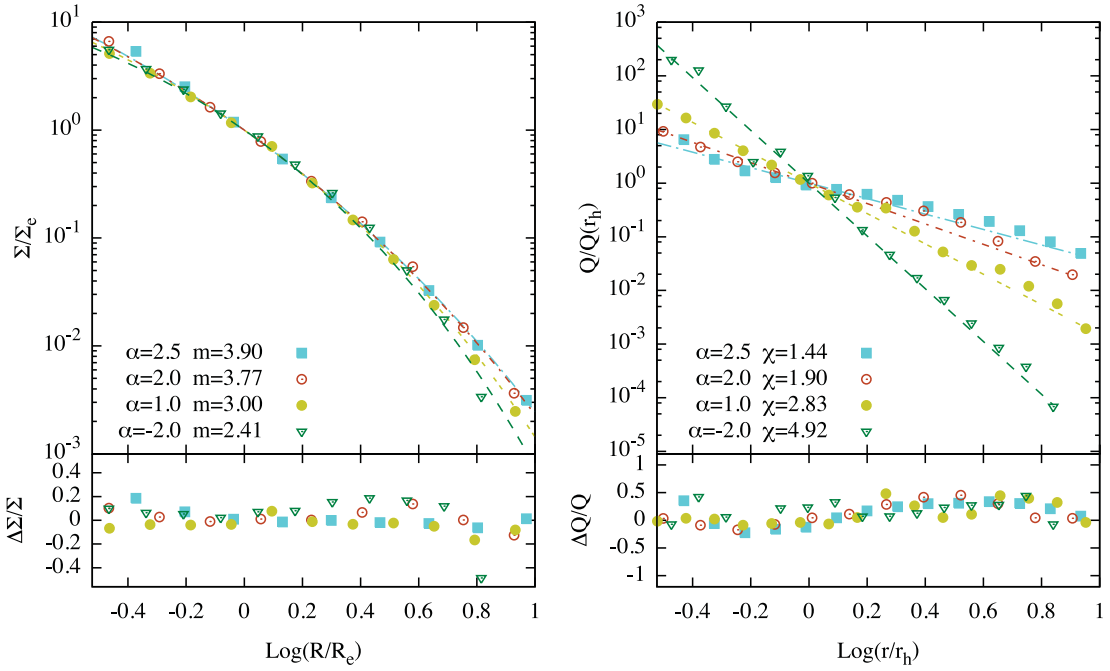

Figure 5. Left: projected density profiles of the end-products of Hernquist initial conditions with $\eta_0 = 0$ and different values of α (dots). The dashed lines represent their Sérsic best fit. Right: the associated pseudo-phase-space density. Residuals with respect to the best fit are also shown.

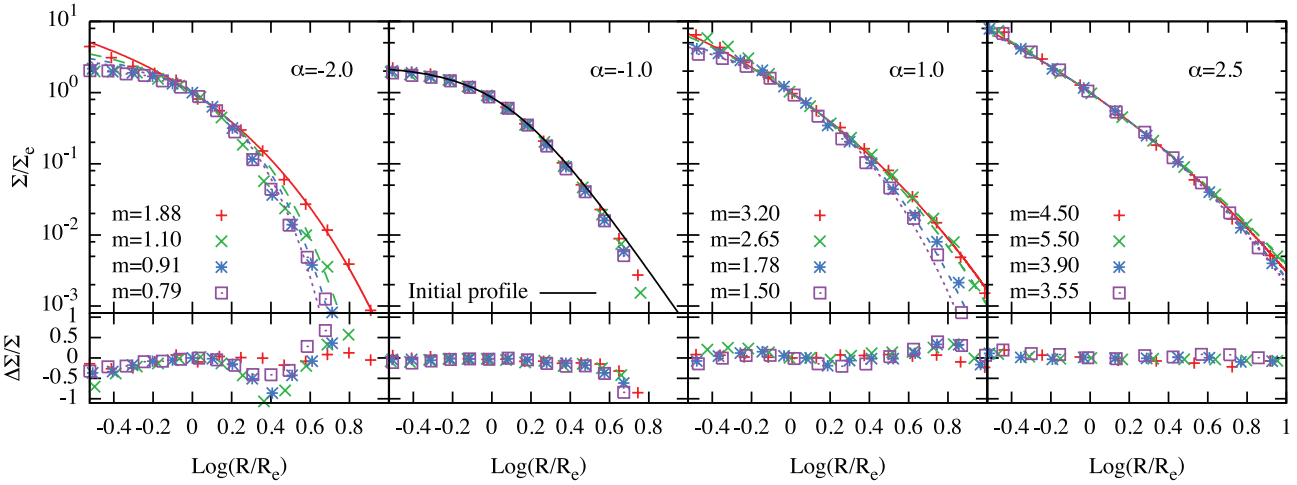

Figure 6. Projected density profiles of the end-products at 50 t_* (points) and their Sérsic best fits (lines) of Plummer initial conditions for $\alpha = -2, -1, 1, 2.5$ and different values of η_0. In the $\alpha = -1$ case (harmonic force), the projected density profile is scale invariant, as expected. The symbols are the same as in Fig. 1.

Ciotti 1991; Binney & Tremaine 2008) corresponding to particles in the outer regions. Note also that how $n(E)$ evolves significantly due to relaxation, with major changes at high energies. For harmonic-like forces the situation is different, and very little evolution is found. Both the initial conditions and the final states have an $n(E)$ distribution peaked at low energies. Of course, consistently with the extraordinary nature of the harmonic force, the $n(E)$ for the $\alpha = -1$ case is not evolving (barring numerical fluctuations). In general, different values of η_0 in the range explored do not affect significantly the shape of the $n(E)$ with the exception of $\alpha = 1$ forces. The systems with $\alpha = 1$ show an intermediate behaviour, with a trend similar to dMOND collapses (see N07a, fig. 5 therein). For this latter case, it is apparent how decreasing values of η_0 tend to populate the external regions of the final systems. As discussed in the Introduction, a specific feature of the $n(E)$ obtained in Newtonian collapses is the exponential shape over some energy range. Here, due to the energy sign associated with the value of α (see discussion in Section 2), we consider the function

$$n(E) = A \times \begin{cases} \mathrm{e}^{-\theta|E|}, & \alpha > 1; \\ \mathrm{e}^{-\theta E}, & \alpha \leq 1, \end{cases} \tag{21}$$

where θ and A are an inverse (positive) temperature and a normalization factor, respectively. It is apparent that for $\alpha < 1$ the shape of $n(E)$ cannot be described by a single-temperature exponential distribution, independently of the hotness of the initial conditions. Instead, for gravity-like forces with $\alpha \geq 1$, a larger energy range exists over which $n(E)$ can be qualitatively described with an

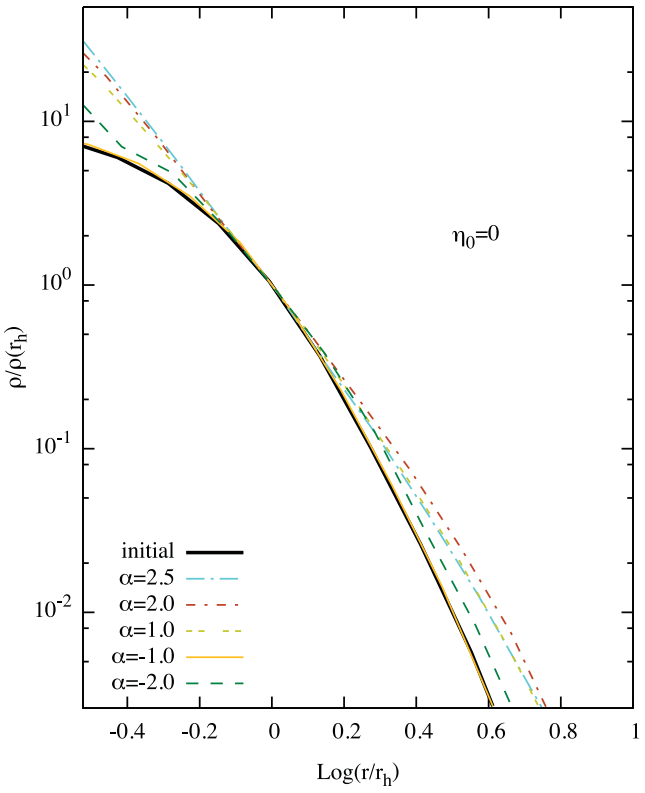

Figure 7. Normalized angle averaged three-dimensional density profiles of the end-products of Plummer initial conditions (black solid line) with $\eta_0 = 0$, and different values of α. Radii are normalized to the volumetric half-mass radius of the final state.

exponential function as in equation (21). The main difference in the gravity-like forces is between the $\alpha = 1$ case and the other case with $\alpha > 1$ (see also Fig. 1): while in the forces allowing for escape ($\alpha > 1$) the exponential region is peaked towards high energies, in the $\alpha = 1$ case the peak is at low energies, corresponding to the central regions. Interestingly, for $\alpha \geq 1$ the trend between the Sérsic index m and the inverse temperature θ of the best-fitting $n(E)$ is qualitatively similar to what found by Ciotti (1991) in the analysis of the Newtonian Sérsic models. We finally note how the current N-body simulations produced final $n(E)$ much better described by an exponential distribution than in the shell model (DCC11), a natural consequence of a better energy exchange among the components of the system. For the final states of the systems with $\alpha > 1$, we also considered the fraction of escapers (i.e. particles having positive energy, see also Joyce, Marcos & Sylos Labini 2009; Sylos Labini 2013). As expected, at fixed α and for given initial density profile, for low values of η_0 (i.e. colder initial conditions) there is a larger number of escapers. Also, for fixed density profile and η_0, the fraction of escapers is found to be weakly dependent on the value of α, with values $\simeq$3 per cent for most cases and with the maximum value of $\simeq$8 per cent for perfectly cold Plummer model with $\alpha = 2.5$.

Another property of interest, recently the focus of several investigations, is the so-called pseudo-phase-space density (e.g. see Taylor & Navarro 2001; Ascasibar & Binney 2005; Hansen, Juncher & Sparre 2010; Ludlow et al. 2010; Barber et al. 2012; Sparre & Hansen 2012) defined as

$$Q = \frac{\rho(r)}{\sigma^3(r)}, \tag{22}$$

where $\rho(r)$ and $\sigma(r)$ are the angle-averaged density and velocity dispersion at radius r. For Newtonian collapses, the numerical simulations have unequivocally shown that Q is described quite well by a power law

$$Q \propto r^{-\chi}, \quad \chi \simeq 1.87. \tag{23}$$

Neither the origin of this relationship nor the dependence of this property on the initial conditions are yet fully understood despite the numerous efforts. The results of numerical simulations seem to point out to a remarkable robustness of equation (23): even though the power-law trend of Q was initially considered a peculiarity of the NFW profiles (Navarro, Frenk & White 1997), it is known that other profiles share this property (e.g. the family of self-consistent f_∞ models, see Bertin & Stiavelli 1984; Zocchi 2010). However, there are self-consistent equilibrium systems where Q is not a power law (e.g. the Plummer sphere). Therefore, it is natural to ask whether the power law is a specific feature of violent relaxation in Newtonian gravity or its origin should be searched more in the physics of dissipationless collapse, independently of the force law involved. Here, we are in the ideal position to address this question, and in

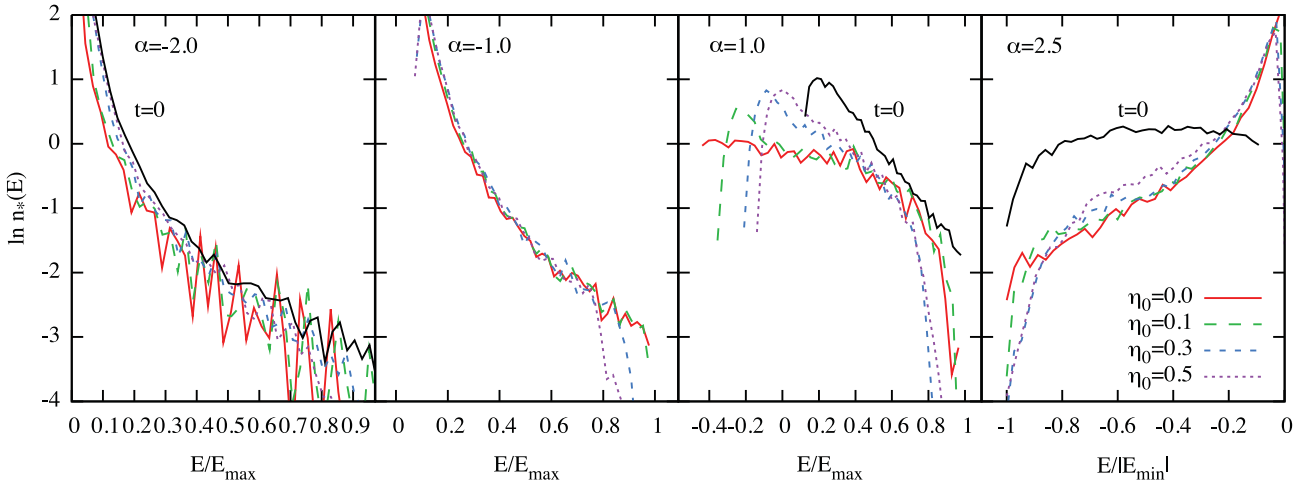

Figure 8. Normalized differential energy distribution $n_*(E) = n(E)/N$ of the end-products of Plummer initial conditions for different values of η_0 and $\alpha = -2, -1, 1, 2.5$. The reference energy is E_{max} or $|E_{min}|$ if $\alpha \leq 1$ or $\alpha > 1$, respectively. The Newtonian case ($\alpha = 2$) is shown in Fig. 1. The heavy solid lines represent the $n_*(E)$ for the initial condition with $\eta_0 = 0$. Hernquist initial conditions lead to very similar energy distributions.

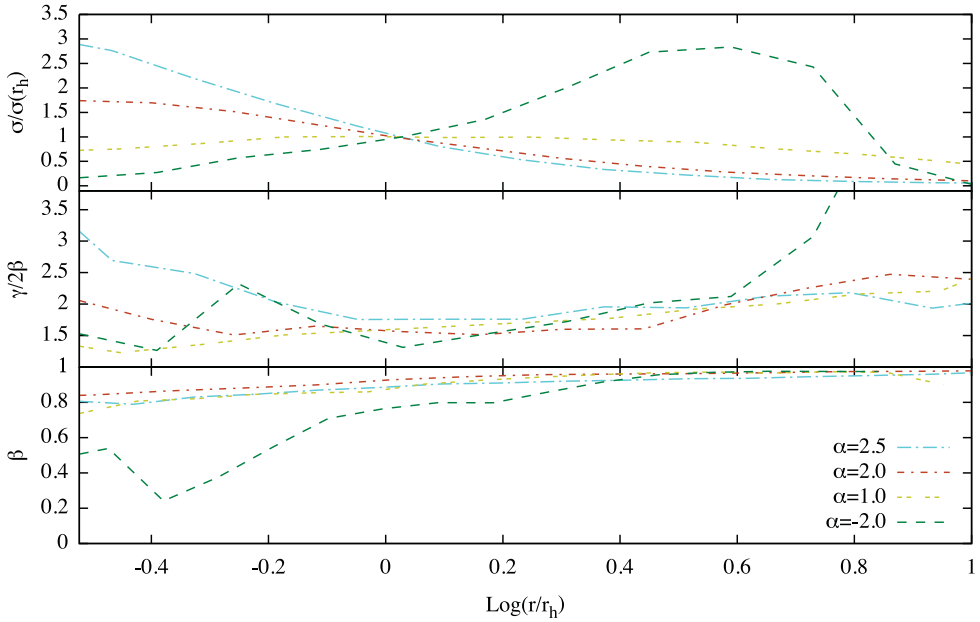

Figure 9. Radial profiles of the angle-averaged velocity dispersion (top), GDSAI indicator (middle) and anisotropy parameter (bottom), for the final virialized states of cold ($\eta_0 = 0$) Hernquist initial conditions. r_h is the volumetric half-mass radius of the final states. Similar trends are found also for larger values of η_0 and for Plummer initial conditions. Note the peculiar off-centre maximum of σ in the superharmonic force case.

fact the obtained results are quite significant. As can be seen in Fig. 5 (right-hand panel) a power-law trend for Q is reproduced surprisingly well also in the case of non-Newtonian forces. For all the considered casees (with the exception of $\alpha = -1$), and independently of the initial density profile, at fixed η_0 the exponent χ increases for decreasing α and the function Q steepens. We also found that at fixed α, Q steepens for decreasing η_0. These findings lead us to conclude that a power-law radial dependence of Q is more a consequence of violent relaxation than of the Newton gravity law.

Finally, we check if the (angle-averaged) GDSAI is obeyed by the end-products for different values of α. Ciotti & Morganti (2010a,b), prompted by the important asymptotic result of An & Evans (2006), proved that a very large class of Newtonian stellar systems with positive phase-space distribution function, necessarily obey the inequality

$$\gamma(r) \geq 2\beta(r), \quad \forall r \tag{24}$$

where

$$\gamma = -\frac{\mathrm{d}\ln\rho}{\mathrm{d}\ln r} \tag{25}$$

is the logarithmic density slope and

$$\beta = 1 - \frac{\sigma_\mathrm{t}^2}{2\sigma_\mathrm{r}^2} \tag{26}$$

is the usual anisotropy parameter (Binney & Tremaine 2008). In the formula above, σ_r and σ_t are the radial and tangential component of the velocity dispersion tensor, respectively. In particular, Ciotti & Morganti (2010b) speculated about a possible universality the GDSAI, even though their analytical methods were unable to treat the cases with $\beta(0) > 1/2$. Significant progress and clarification has been made in the subject (van Hese et al. 2011; An et al. 2012) and now the case of systems with *separable augmented density* is well understood: the GDSAI is obeyed by all separable systems with $\beta(0) \leq 1/2$, while counterexamples exist for systems with $\beta(0) > 1/2$. Much less is known about systems with non-separable augmented density, but numerical simulations in Newtonian gravity seem to suggest that also in general systems the GDSAI is usually satisfied. Here, we analysed the results of the simulations for different values of α and η_0. The trends of γ and β, obtained using spherical averages and excluding the innermost regions (where discreteness effects dominate), revealed that the final states obey the GDSAI (with the obvious exception of the harmonic oscillator force). This is shown in Fig. 9 where, even in presence of numerical noise, it is apparent that overall $\gamma \geq 2\beta$, reinforcing the idea that the physical process leading to the establishment of the GDSAI may be independent of the specific force law considered. Finally, from the bottom panel of Fig. 9, it is also interesting to note that how the final systems are significantly radially anisotropic in their outer regions, and become more and more isotropic near the centre, as also commonly found in Newtonian simulations. The $\alpha = -2$ case stands out as the less anisotropic and it is curious to recall that these systems are also those for which the Sérsic law provides the less satisfactory description (Fig. 6).

5 DISCUSSION AND CONCLUSIONS

As discussed in the Introduction, several theoretical arguments point towards the importance of elucidating the process of dissipationless collapse and virialization of N-body systems with additive interparticle forces proportional to $r^{-\alpha}$, a generalization of the Newtonian force. For this task, we built a direct N-body code: preliminary results obtained with a shell model in spherical symmetry (DC09; DCC11) appear to be confirmed by the present simulations. The main results can be summarized as follows.

The relaxation process, independently of the initial density profile (Hernquist or Plummer), is characterized by a first phase of strong oscillations of the virial ratio, followed by a gentler phase of relaxation. For decreasing α, the peak value of the virial ratio increases reaching a value formally infinite in the case of a perfectly cold collapse with $\alpha = -1$ (i.e. a system of harmonic oscillators), and then decreases again. This non-monotonic behaviour is a

consequence of the different degrees of phase mixing as a function of α. Qualitatively, this effect can be understood by considering the force field inside a shell of matter for different values of α. As expected, systems with $\alpha = -1$ do not relax due to their extraordinary orbital structure in which each particle behaves as an isolated harmonic oscillator (e.g. Lynden-Bell & Lynden-Bell 2008).

With the obvious exception of the $\alpha = -1$ force, when the systems retain their initial spherical shape, the final states are triaxial. As a rule triaxiality increases for colder initial conditions, similarly to what happens in Newtonian collapses. However, for fixed initial virial ratio η_0, triaxiality is not a monotonic function of α: for decreasing α the flattening increases, reaches a maximum and then decreases again. The value of α for which the triaxiality is maximum depends on η_0, but it is almost independent of the initial density profile. Remarkably, no models are found to be flatter than an elliptical galaxy of type E7, independently of α and η_0.

In general, the Sérsic law provides a good description of most of the final states, with large Sérsic index m associated with large values of α (i.e. for gravity-like forces), and with cold initial conditions. Hotter initial conditions and harmonic-like forces produce density profiles characterized by smaller m. Moreover, the quality of the Sérsic fit deteriorates for low values of α.

The differential energy distribution $n(E)$ of the final states shows two distinct behaviours, separated by the case $\alpha = 1$. In particular, $n(E)$ is well described over a large range of energies by an exponential function peaked at high energies for gravity-like forces with $\alpha > 1$. For $\alpha = 1$, the final $n(E)$ is also exponential, but now the distribution is peaked at low energies (as in MOND simulations; N07a). Finally, when $\alpha < 1$, very little evolution is found, and $n(E)$ remains peaked at low energies. Remarkably, for $\alpha \geq 1$ the trend of the inverse temperature θ with the Sérsic index m is similar to what found for the Newtonian Sérsic models, with θ increasing for decreasing m (Ciotti 1991).

We found that the pseudo-phase-space density $Q = \rho/\sigma^3$ of the (angle-averaged) final states is described very well by a power law of radius $r^{-\chi}$, over a large radial range. In general, Q steepens for decreasing α, while at fixed α it flattens for increasing values of η_0. In addition, we also found that the GDSAI holds (well within numerical uncertainties) for all the virialized end-states, and the amount of radial anisotropy tends to be higher for $\alpha > 0$ (i.e. for gravity-like force) than for $\alpha < 0$.

Overall the main conclusion of the present study is that several structural and dynamical features of the virialized states of cold and dissipationless collapses are not restricted to the special nature of the Newton law, but they appear to be more a property of the long-range forces. Among the radial $r^{-\alpha}$ forces, however, the gravity-like forces ($\alpha > 0$) are those with the results more similar to the $1/r^2$ force. In addition, we found that the systems with interparticle force proportional to $1/r$ behave in many respects as dMOND systems. In particular, we confirmed that the relaxation time (in units of the internal dynamical time) is longer for $\alpha = 1$ than for $\alpha = 2$, and this is due to the force becoming more similar to the harmonic oscillator case ($\alpha = -1$) when the system oscillates forever. Future explorations, exploiting the similarity between $1/r$ and dMOND forces, will be focused on the study of radial orbit instability for $1/r^\alpha$ forces, in the line of the MOND study of Nipoti, Ciotti & Londrillo (2011).

ACKNOWLEDGEMENTS

We thank Steen Hansen, Alberto Parmeggiani and the anonymous referee for useful comments. LC and CN acknowledge financial support from PRIN MIUR 2010-2011, project 'The Chemical and Dynamical Evolution of the Milky Way and Local Group Galaxies', prot. 2010LY5N2T. This material is based upon work supported in part by the National Science Foundation under grant No. 1066293 and the hospitality of the Aspen Center for Physics.

REFERENCES

An J. H., Evans N. W., 2006, ApJ, 701, 1500
An J. H., van Hese E., Baes M., 2012, MNRAS, 422, 652
Andredakis Y. C., Peletier R. F., Balcells M., 1995, MNRAS, 275, 874
Ascasibar Y., Binney J., 2005, MNRAS, 356, 872
Barber J. A., Zhao H., Wu X., Hansen S. H., 2012, MNRAS, 424, 1737
Bekenstein J., Milgrom M., 1984, ApJ, 286, 7
Bertin G., Stiavelli M., 1984, A&A, 137, 26
Bertin G., Trenti M., 2003, ApJ, 584, 729
Bertin G., Ciotti L., Del Principe M., 2002, A&A, 386, 149
Binney J., 1982, MNRAS, 200, 951
Binney J., Tremaine S., 2008, Galactic Dynamics, 2nd edn. Princeton Univ. Press, Princeton, NJ
Bouchet F., Gupta S., Mukamel D., 2010, Physica A, 389, 4389
Brandao C. S. S., de Araujo J. C. N., 2012, ApJ, 750, 29
Caon N., Capaccioli M., D'Onofrio M., 1993, MNRAS, 265, 1013
Chavanis P. H., 2008, in Campa A., Giansanti A., Morigi G., Sylos-Labini F., eds, AIP Conf. Proc. Vol. 970, Dynamics and Thermodynamics of Systems with Long-Range Interactions: Theory and Experiments. Am. Inst. Phys., New York, p. 39
Ciotti L., 1991, A&A, 249, 99
Ciotti L., 2000, Lecture Notes on Stellar Dynamics. Scuola Normale Superiore, Pisa
Ciotti L., 2009, Riv. Nuovo Cimento, 32, 1
Ciotti L., Bertin G., 1999, A&A, 352, 447
Ciotti L., Morganti L., 2010a, MNRAS, 401, 1091
Ciotti L., Morganti L., 2010b, MNRAS, 408, 1070
Ciotti L., Nipoti C., Londrillo P., 2007, in Bertin G., Pozzoli R., Romé M., Srinivasan K. R., eds, Proc. Int. Workshop, Collective Phenomena in Macroscopic Systems. World Scientific Press, Singapore, p. 177
Courteau S., de Jong R. S., Broeils A. H., 1996, ApJ, 437, 21
Dehnen W., 2001, MNRAS, 324, 273
Di Cintio P. F., 2009, Master thesis, Bologna Univ. (DC09)
Di Cintio P. F., Ciotti L., 2011, Int. J. Bifurcation Chaos, 21, 2279 (DCC11)
Gabrielli A., Joyce M., Marcos B., 2010, Phys. Rev. Lett., 105, 210602
Gerhard O. E., Spergel D. N., 1992, ApJ, 397, 38
Graham A., 1998, MNRAS, 293, 933
Graham A., Colless M., 1997, MNRAS, 287, 221
Hansen S. H., Moore B., 2006, New Astron., 11, 333
Hansen S. H., Juncher D., Sparre M., 2010, ApJ, 718, 68
Hénon M., 1964, Ann. Astrophys., 27, 83
Hernquist L., 1990, ApJ, 356, 359
Joyce M., Worrakitpoonpon T., 2011, Phys. Rev. E., 84, 1139
Joyce M., Marcos B., Sylos Labini F., 2009, MNRAS, 397, 775
Kandrup H. E., 1989, Phys. Rev. A., 40, 7265
Londrillo P., Nipoti C., 2009, Mem. Soc. Astron. Ital. Suppl., 13, 89
Londrillo P., Messina A., Stiavelli M., 1991, MNRAS, 250, 54
Londrillo P., Nipoti C., Ciotti L., 2003, Mem. Soc. Astron. Ital. Suppl., 1, 18
Ludlow A. D., Navarro J. F., Springel V., Vogelsberger M., Wang J., White S. D. M., Jenkins A., Frenk C. S., 2010, MNRAS, 406, 137
Lynden-Bell D., 1967, MNRAS, 136, 101
Lynden-Bell D., Lynden-Bell R. M., 2008, J. Stat. Phys., 117, 199
Malekjani M., Rahvar S., Haghi H., 2009, ApJ, 694, 1220
Malekjani M., Haghi H., Jassur D. M. Z., 2012, New Astron., 17, 149
Marcos B., Gabrielli A., Joyce M., 2012, Cent. Eur. J. Phys., 10, 676
Meza A., Zamorano N., 1997, ApJ, 490, 136
Milgrom M., 2010, MNRAS, 403, 886
Mineau P., Feix M. R., Rouet J. L., 1990, A&A, 228, 344
Moffat J. W., Sokolov I. Yu., 1996, Phys. Lett. B, 378, 59

Navarro J. F., Frenk C. S., White S. D. M., 1997, ApJ, 490, 493
Nipoti C., Londrillo P., Ciotti L., 2002, MNRAS, 332, 901
Nipoti C., Londrillo P., Ciotti L., 2006a, MNRAS, 370, 681 (N06a)
Nipoti C., Londrillo P., Ciotti L., 2006b, in Voli M., Coluccia P., eds, Science and Supercomputing at CINECA, Bologna, Italy, p. 122 (N06b)
Nipoti C., Londrillo P., Ciotti L., 2007a, ApJ, 660, 256 (N07a)
Nipoti C., Londrillo P., Ciotti L., 2007b, MNRAS, 381, 107
Nipoti C., Ciotti L., Londrillo P., 2011, MNRAS, 414, 3298
Plummer H. L., 1911, MNRAS, 71, 460
Prugniel P., Simien F., 1997, A&A, 321, 111
Sanders R. H., 1998, MNRAS, 296, 1009
Sanders R. H., 2008, MNRAS, 386, 1588
Sparre M., Hansen S. H., 2012, J. Cosmol. Astropart. Phys., 10, 49
Srinivasan K., Mahawar H., Sarin V., 2005, in Sunderam V. S. et al., eds, Proc. Int. Conf. Comput. Sci. 05, A Multipole Based Treecode Using Spherical Harmonics for Potentials of the Form r. Springer-Verlag, Berlin, p. 107
Stein E. M., 1970, Singular Integrals and Differentiability Properties of Functions. Princeton Univ. Press, Princeton, NJ
Sylos Labini F., 2013, MNRAS, 429, 679
Takizawa M., Inagaki S., 1997, preprint (arXiv:astro-ph/9702002v1)
Taylor J. E., Navarro J. F., 2001, ApJ, 563, 483
Teles T. N., Levin Y., Pakter R., 2011, MNRAS, 417, 21
Trenti M., Bertin G., 2005, A&A, 429, 161
Trenti M., Bertin G., van Albada T. S., 2005, A&A, 433, 57
Trujillo I., Graham A., Caon M., 2001, MNRAS, 326, 869
van Albada T. S., 1982, MNRAS, 201, 939
van Hese E., Baes M., Dejonghe H., 2011, ApJ, 726, 80
Visbal E., Loeb A., Hernquist L., 2012, preprint (arXiv:astro-ph/1206.5852)
Youngkins V. P., Miller B. N., 2000, Phys. Rev. E, 62, 4583
Zocchi A., 2010, Master thesis, Milano Univ.

This paper has been typeset from a TEX/LATEX file prepared by the author.